RSC Advances

PAPER

View Article Online
View Journal | View Issue

Cite this: *RSC Adv.*, 2017, **7**, 9484

Atmospheric chemical reaction mechanism and kinetics of 1,2-bis(2,4,6-tribromophenoxy)ethane initiated by OH radical: a computational study†

Qi Yu,[a] Hong-Bin Xie,*[a] Tianchi Li,[a] Fangfang Ma,[a] Zihao Fu,[a] Zhongyu Wang,[a] Chao Li,[b] Zhiqiang Fu,[a] Deming Xia[a] and Jingwen Chen[a]

Received 12th November 2016
Accepted 25th January 2017

DOI: 10.1039/c6ra26700a

rsc.li/rsc-advances

The unexpected diverse effect of alternatives for banned chemicals has stimulated scientific and public concern on their environmental risk. As an alternative of polybrominated diphenyl ethers (PBDEs), 1,2-bis(2,4,6-tribromophenoxy) ethane (BTBPE) is currently one of the most commonly applied novel brominated flame retardants with wide market prospects. Due to its frequent and high detection in the atmosphere, revealing the atmospheric fate of BTBPE is of great significance. Here, the mechanism and kinetics of the ·OH-initiated atmospheric reaction of BTBPE have been investigated by combined quantum chemical calculations and kinetics modeling. The results indicate that ·OH addition and hydrogen abstraction pathways in the initiated reactions, are competitive with a rate constant ratio of 3 : 1, and the intermediates formed would react with O_2/NO to finally form peroxy radicals and OH-BTBPE which tends to be more toxic. The calculated overall reaction rate constant is 1.0×10^{-12} cm^3 per molecule per s, translating into 11.8 days atmospheric lifetime of BTBPE. This clarifies that BTBPE as a substitute for PBDEs still has atmospheric persistence.

1. Introduction

Synthetic chemicals have been considered as significant risk sources to human and ecological health according to the United Nations Environment Programme.[1,2] Currently, a series of laws and regulations, such as the Stockholm Convention[3] and REACH (Registration, Evaluation, Authorization and Restriction of Chemicals),[4] have been set up to restrict or ban the use of some hazardous chemicals. To meet the market demand, alternatives for those banned chemicals have been largely and rapidly introduced into markets, lacking a comprehensive risk assessment. However, if we looked back, it was not hard to find that some alternatives, especially those that have similar electronic structure properties to the banned chemicals, have led to unexpected diverse effects.[5] For instance, hydrochlorofluorocarbons, as alternatives of chlorofluorocarbons, have been found to have ozone destruction and global warming effects.[6,7] 4,4′-Methylenediphenol, 4-hydroxyphenyl sulfone and 4,4′-(hexafluoroisopropylidene)diphenol, as substitutes of bisphenol A (BPA), have shown similar or even greater estrogenic and/or antiandrogenic activities than BPA.[5,8] Therefore, to avoid this regrettable substitution, a comprehensive environmental risk assessment for alternatives, especially those that have similar electronic structure properties to the banned chemicals, has to be performed.

As an alternative for polybrominated diphenyl ethers (PBDEs),[9] 1,2-bis(2,4,6-tribromophenoxy)ethane (BTBPE) has similar electronic structure to PBDEs (Fig. 1). BTBPE has been included in the 2007 OECD list of high production volume chemicals and detected in various environmental matrixes, *e.g.* indoor dust, air, sewage sludge, water, snow pits and even in Arctic.[10–25] To probe the environmental risk of BTBPE, studies on the transformation and fate of BTBPE in the environment have recently come out,[11,26–28] concerning whether the transformation of BTBPE can form toxic compounds such as polybrominated dibenzo-*p*-dioxins and polybrominated dibenzofurans (PBDD/Fs) like transformations of other halogenated flame retardants,[28–31] besides the routine toxicological investigation. Zhang *et al.* found that debromination and ether bond cleavage are the main phototransformation pathways for BTBPE in aqueous solution, which leads to the formation of toxic bromophenols.[27] Altarawneh *et al.* observed that thermal decomposition of BTBPE can generate several congeners of brominated diphenyl ethers and their OH/$OCHCH_2$ substituents, which serve as direct precursors for the formation of polybrominated dibenzo-*p*-dioxins.[28] These studies indicated that the transformation of BTBPE could increase environmental

[a]*Key Laboratory of Industrial Ecology and Environmental Engineering, Ministry of Education, School of Environmental Science and Technology, Dalian University of Technology, Dalian 116024, China. E-mail: hbxie@dlut.edu.cn*

[b]*State Environmental Protection Key Laboratory of Wetland Ecology and Vegetation Restoration, School of Environment, Northeast Normal University, Changchun 130117, China*

† Electronic supplementary information (ESI) available: Details of methods and rate calculation, Tables S1–S4, Fig. S1 and S2. See DOI: 10.1039/c6ra26700a

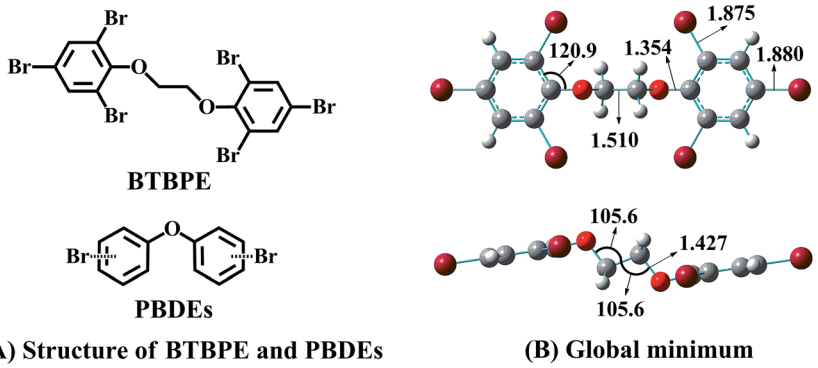

(A) Structure of BTBPE and PBDEs (B) Global minimum

Fig. 1 (A) The structures of BTBPE and PBDEs. (B) PBE1PBE/6-31+G(d,p)-optimized global minimum of BTBPE with important bond lengths in angstroms (Å) and angles in degrees (°).

risk, due to the formation of more toxic products. However, information on the atmospheric fate and transformation of BTBPE is scarce although BTBPE has been frequently and highly detected in the atmosphere.[11,14–19]

As a semivolatile compound, BTBPE can exist in the gas-phase and particle in the atmosphere.[11,14–19] The concentration of BTBPE in particles were detected to be 1–2 times than that in gas-phase in the Great Lakes atmosphere.[19] Therefore, in principle, BTBPE can undergo both gas-phase and heterogeneous transformation. Since the gas-particle partition of BTBPE in the atmosphere is under dynamic equilibrium, part of BTBPE in particles will transfer to gas-phase once gaseous BTBPE is transformed. Therefore, gas-phase transformation could be also important although more BTBPE was detected in particles.[19] In addition, the information on gaseous transformation of BTBPE should provide a foundation for the future study on heterogeneous one of BTBPE. Considering ·OH initiated oxidation is a dominating removal pathway for PBDEs and most organic pollutants in the atmosphere,[32–34] we supposed such oxidation also plays an important role in BTBPE gas-phase transformation.

In this study, we investigated the reaction mechanism and kinetics of BTBPE initiated by ·OH using a combination of quantum chemistry calculations and kinetic modeling. The study includes the reaction mechanism and kinetics of BTBPE + ·OH and subsequent reactions consisting of isomerization, dissociation, and bimolecular reactions with O_2/NO. This study is of significance for understanding the fate and environmental risk of BTBPE and other alternatives with similar structures to banned chemicals.

2. Computational details

2.1. *Ab initio* electronic structure calculations

All the electronic structure and energy calculations were carried out with Density Functional Theory (DFT) method within the GAUSSIAN 09 program package.[35] The advantage of DFT lies in its competitive accuracy/cost ratio. However, before being used to predict accurate kinetics for the target system, specific DFT methods need to go through an assessment step by a comparison with higher-level theoretical approaches (*e.g.*, CCSD(T)) or, if available, accurate experimental results. After carefully testing DFT methods on our target system, PBE1PBE and M06-2X functional were selected.[36,37] The details for the test were presented in (ESI†). Exactly, all reaction pathways except H-abstractions in ·OH initiated reactions were investigated by PBE1PBE functional, while the H-abstractions in ·OH initiated reactions were investigated by M06-2X functional. The geometry optimizations and harmonic frequency calculations of the reactants, products, intermediates and transition states were performed using the PBE1PBE/M06-2X method with the 6-31+G(d,p) basis set. Transition states were verified to connect designated local minimum using intrinsic reaction coordinate (IRC) calculations at the theoretical level for corresponding geometry optimizations. Single-point energy calculations were performed at PBE1PBE/6-311++G(3df,2pd) or M06-2X/6-311++G(3df,2pd) level with zero-point correction at the theoretical level for corresponding geometry optimizations.

2.2. Kinetics calculations

All reaction rate constants were calculated by the MultiWell-2014.1 master equation code.[38–41] The MultiWell program employs Rice–Ramsperger–Kassel–Marcus (RRKM) theory to compute energy-dependent microcanonical rate constants for reactions based on sums and densities of states for the PBE1PBE/6-31+G(d,p) or M06-2X/6-31+G(d,p) structures and the PBE1PBE/6-311++G(3df,2pd) or M06-2X/6-311++G(3df,2pd) barrier heights.[42] Tunneling correction has been included in the microcanonical rate constant calculation by using one dimensional unsymmetrical Eckart barrier.[43] The energy-grained master equation was solved over 2000 grains of 10 cm^{-1} each, carried on to 85 000 cm^{-1} for the continuum component of the master equation. N_2 gas was used as the buffer gas, and the collision transfer was treated using the conventional exponential-down model with $\Delta E_d = 200$ cm^{-1}. The Lennard-Jones parameters for intermediates were calculated from an empirical method proposed by Gilbert and Joback *et al.*[44,45] The rate constants for the barrierless entrance pathways were calculated by the restricted Gorin model when the experimental rate constant for a target system or its similar one is available or by the long-range transition state theory when there is no related experimental data.[46,47] This scheme had been

successfully used in our previous study.[48] The details for the reaction rate constant calculations with the restricted Gorin model and long-range transition state theory were presented in the ESI.†

2.3. Global minimum search

The reactant BTBPE has conformational degrees of freedom that may influence the calculated reaction mechanism and kinetics. Here, global minimum of BTBPE was selected as its starting reactant. *Ab initio* molecular dynamics (AIMD) was used to generate reasonable gas-phase conformations for BTBPE by employing the BLYP functional on def2-SVP basis set with dispersion correction.[49] In order to sample a large number of different conformations in a short time, the simulation temperature was set to 500 K. The total length of AIMD simulation was 5000 time steps with each step of 2 fs. AIMD simulations were performed within TURBOMOLE program package.[50] We selected the conformations from the AIMD run as the starting point to obtain different local minimum structures at PBE1PBE/6-31+G(d,p) level. Single-point energy calculations were further performed at PBE1PBE/6-311++G(3df,2pd) level. The conformer with the lowest Gibbs free energy (G) value was identified as the global minimum. All structures of the conformers and relative Gibbs free energies values are presented in Table S1 of ESI.†

3. Results and discussion

3.1. Global minimum of BTBPE

The global minimum of BTBPE was depicted in Fig. 1B. It exhibits an approximate C_{2h} symmetry, with root-mean-square deviation (RMSD) value 0.006 to corresponding strict C_{2h} symmetry structure. Therefore, the approximate symmetrical sites of BTBPE could have similar reactivity toward ·OH due to their similar chemical environment. It deserves mentioning that strict C_{2h} symmetry structure was identified with one imaginary frequency.

3.2. Initial reactions with ·OH

Generally, the reactions of organic pollutants with ·OH mainly proceed *via* either addition of ·OH to unsaturated bonds or H-abstraction. Therefore, ·OH may add to π bond of phenyl group or abstract H-atom from ethyl group and phenyl group in the reaction of BTBPE with ·OH. Totally, BTBPE has 2 phenyl groups and 8H-atoms, therefore, it has 12 different addition positions and 8H-abstraction sites for the attack by ·OH. The possible addition and H-abstraction pathways for the reactions of BTBPE with ·OH are depicted in Fig. 2, and the optimized geometries for some important transition states and intermediates are presented in Fig. 3. Each reaction pathway proceeds through a pre-reactive complex and H-abstraction pathways also proceed through a post-reactive complex. It deserves mentioning that the C–Br bond is broken when ·OH add to CBr site to form IM2 + Br, IM6 + Br, IM2′ + Br and IM6′ + Br. However, C–Br bond is kept although CBr bond length become longer (from 1.875 Å to 2.055 Å) during ·OH addition to CBr site to form IM4 and IM4′. The calculated relative energy (to the reactants) of pre-reactive complex (ΔE_{RC}) and post-reactive complex (ΔE_{PC}), activation energy values (ΔE_a) and activation free energy values ($\Delta G^{\ddagger}$) are listed in Table 1.

It can be seen from Table 1 that the ΔE_a values for additions occurring at the CH sites of 2,4,6-tribromophenoxy group *via* transition states TS3, TS3′, TS5 and TS5′ to form IM3, IM3′, IM5 and IM5′, and H-abstractions from –O–CH_2–CH_2–O– *via* transition states TS7-1, TS7′-1, TS7-2 and TS7′-2 to form IM7-1 + H_2O, IM7′-1 + H_2O, IM7-2 + H_2O and IM7′-2 + H_2O, are comparable and much lower than those of other pathways. Therefore, initial reaction of BTBPE with ·OH mainly form IM3, IM3′, IM5, IM5′, IM7-1, IM7′-1, IM7-2 and IM7′-2.

Based on ΔE_a values for all reaction pathways, we discuss the reactivity trend of addition sites and H-abstraction sites of BTBPE toward ·OH. The reaction sites with the higher ΔE_a values will have the lower reactivity toward ·OH. Therefore, the reactivity of addition sites follows the order of the CH sites > CO sites > CBr sites of 2,4,6-tribromophenoxy group of BTBPE. We noted that previous study found that ·OH additions to CBr site tend to have a higher E_a value than those of addition to CH sites of bromophenoxy group in the reaction of PBDEs with ·OH.[33,34,51,52] This agrees with our findings. The C–H of 2,4,6-tribromophenoxy group has lower H-abstraction reactivity than that of –O–CH_2–CH_2–O– group. According to the C–H bond dissociation energy in C_6H_6 (112.9 ± 0.5 kcal mol^{-1}) and CH_3OCH_3 (95.3 kcal mol^{-1}),[53] we speculate that CH bond dissociation energy in 2,4,6-tribromophenoxy group is higher than that in –O–CH_2–CH_2–O– group, which can explain lower H-abstraction reactivity in 2,4,6-tribromophenoxy group than that in –O–CH_2–CH_2–O– group. It deserves mentioning that variation tendency of ΔE_a is consistent with that of $\Delta G^{\ddagger}$ (Table 1), indicating that the entropy effect can't change the energy order of different pathways. Details of activation enthalpy values ($\Delta H^{\ddagger}$) and activation entropy ($\Delta S^{\ddagger}$) for all pathways were shown in Table S2.† In addition, approximate symmetrical sites have (almost) the same ΔE_a values toward ·OH, *e.g.* 1 and 1′, 2, 6, 2′ and 6′, 3, 5, 3′ and 5′, 4 and 4′, 7-1, 7-2, 7-1′ and 7-2′, respectively. Therefore, in the following discussion, only one site (1, 2, 3, 4, 7-1 and 3-H) among all symmetrical sites was considered.

3.3. Kinetics

The master equation method was used to calculate the reaction rate constants for the reaction of BTBPE + ·OH, including pathways to form IM1, IM2, IM3, IM4, IM7-1 and IM3-H. Moreover, due to the barrierless pre-reactive complexes and post-reactive complex, we performed the long-range transition state theory to calculate the formation rate constant of pre-reactive complexes and post-reactive complex for the reaction BTBPE + ·OH. The overall reaction rate constant was calculated to be sum of all sites by assuming that approximate symmetrical sites have the same reaction rate constants. The values of k_{OH} and Γ for the reaction of BTBPE with ·OH at 298 K are presented in Table 2. To further evaluate the effect of temperature (T) and pressure (P) on k_{OH}, $k_{(T,P)}$, k_{OH} as a function of T and P, was calculated for the overall reaction and two favorable pathways forming IM3 + IM3′ + IM5 + IM5′ and IM7-1 + IM7-2 + IM7′-1 + IM7′-2 at temperature range

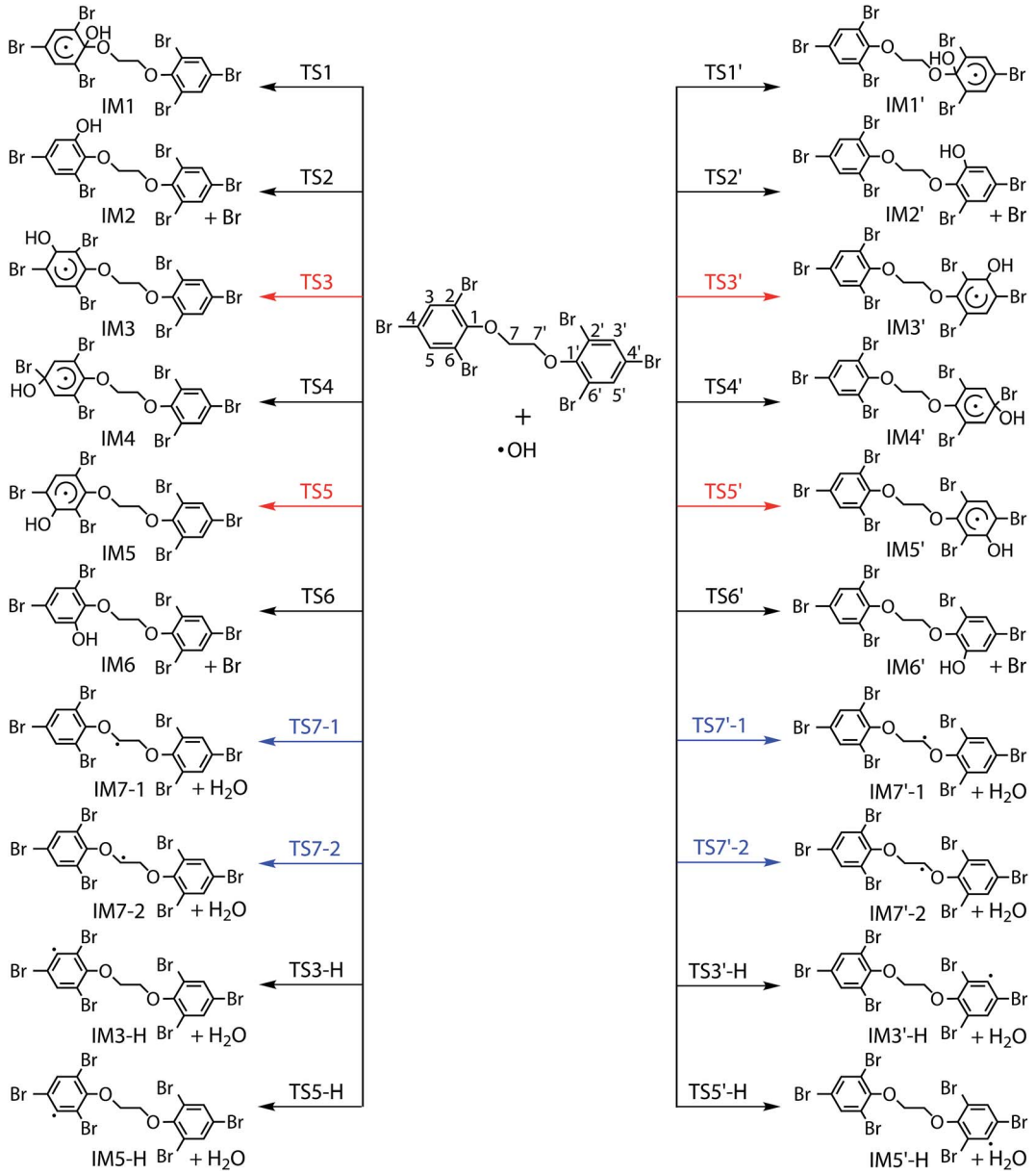

Fig. 2 Addition and H-abstraction pathways for the reaction of BTBPE with ·OH. The symbols "TSm/TSm-H" and "IMm/IMm-H" denote the transition states and intermediates involved in the reaction, respectively, in which m denotes different reaction sites.

270–330 K and pressure range 81–122 kPa (shown in Fig. S1†). As seen in Fig. S1,† $k_{(T,P)}$ presents a negative temperature dependence but no obvious pressure dependence for both the overall reaction and considered two favorable pathways. The overall rate constant was calculated to be 1.0×10^{-12} cm^3 per molecule per s at 298 K and 101 kPa, which is about 20 times higher than that of (5.2×10^{-14} cm^3 per molecule per s) of 2,2′,4,4′,5-pentabrominated diphenyl ether (BDE99).[52] The calculated branching ratio Γ value for the addition products IM3 + IM3′ + IM5 + IM5′ is 73.5% and H-abstraction products IM7-1 + IM7-2 + IM7′-1 + IM7′-2 is 24.9% at 298 K, which are much higher than those for other addition and H-abstraction pathways. Therefore, CH site addition of 2,4,6-tribromophenoxy group and H-abstraction from –O–CH_2–CH_2–O– group are the most favorable pathways for the reaction BTBPE + ·OH.

3.4. Subsequent reactions of primary intermediates

The chemically activated intermediates/products produced in the initial reaction can subsequently isomerize, dissociate or react with atmospheric O_2. Here, we focus primarily on the further transformation of the intermediates with higher Γ values *i.e.* intermediates from addition IM3, IM3′, IM5 and IM5′ and from H-abstraction IM7-1, IM7-2, IM7′-1 and IM7′-2. In addition, based on the consideration of approximate molecular symmetry as mentioned above, only the transformations of IM3 and IM7-1 were investigated.

Isomerization and dissociation. Similar to the reactions of aromatics with ·OH, the formed IM3 can occur H-shift (to CBr site) and H-dissociation. Considered H-shift and H-dissociation pathways with their corresponding ΔE_a and $\Delta G^{\ddagger}$ values are

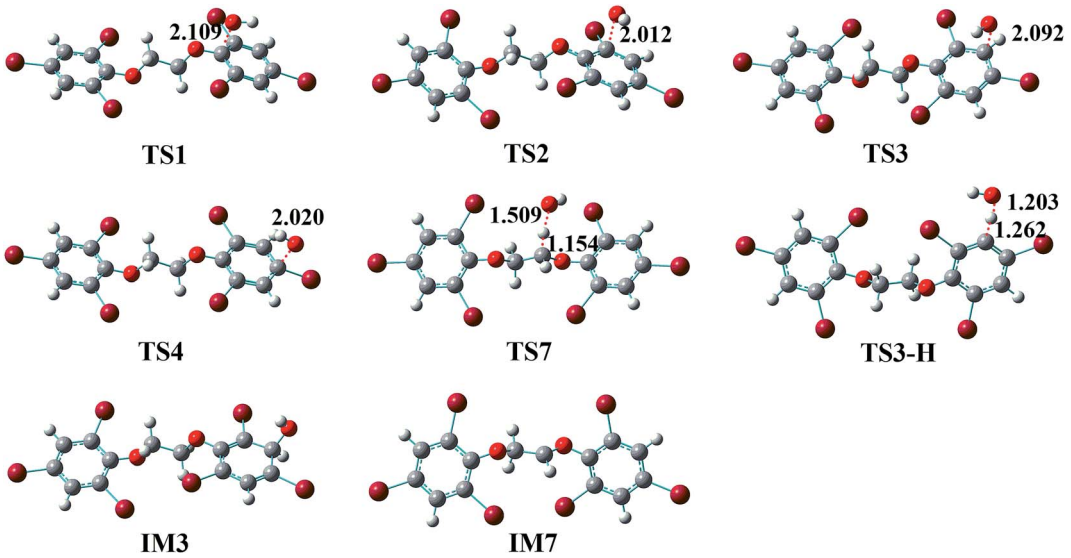

Fig. 3 PBE1PBE/6-31+G(d,p) or M06-2X/6-31+G(d,p)-optimized geometries for some important transition states and intermediates involved in the reaction of BTBPE + ·OH. The distances are in angstroms (Å).

presented in Fig. 4A, and their unimolecular rate constants are listed in Table S3.† It deserves mentioning that the H-shift simultaneously leads to the break of C–Br bond. The ΔE_a values for H-shift and H-dissociation pathways are 41.7 kcal mol^{-1} and 27.6 kcal mol^{-1}, corresponding to unimolecular rate constants in the order of 10^{-18} s^{-1} and 10^{-8} s^{-1}, respectively. Therefore, the isomerization and dissociation reactions of IM3 proceed slowly. As for IM7-1, four possible pathways (Fig. 4B) were considered including Br-shift to form P3, H-dissociation to form P4, phenyl C–O bond rupture to form P5 and P6, and alkyl C–O bond rupture to form P7 and P8. The last process needs to overcome 10.5 kcal mol^{-1} energy barrier, corresponding to rate constant 3.3×10^4 s^{-1}. However, ΔG values of products for the former three pathways are >0, indicating thermodynamical unfeasibility.

Reaction with O_2. Intermediates IM3 and IM7-1 should react with atmospheric O_2, the most abundant oxidants in the earth's atmosphere. All possible pathways for both reactions IM3 + O_2 and IM7-1 + O_2 are presented in Fig. 5A and B, respectively, and optimized geometries of some important

Table 1 Calculated relative energy (to the reactants) of pre-reactive complex (ΔE_{RC}) and post-reactive complex (ΔE_{PC}), activation energy values (ΔE_a) and activation free energy values ($\Delta G^{\ddagger}$) for the reaction BTBPE + ·OH (unit is in kcal mol^{-1})

Pathways	Species[a]	Sites[a]	ΔE_{RC}[b]	ΔE_a[b]	$\Delta G^{\ddagger}$[b]	ΔE_{PC}[b]
Addition to phenyl group	IM1	CO	−0.5	0.9	9.7	—
	IM1′	CO	−0.5	0.9	9.7	—
	IM2	CBr	−0.9	4.2	13.9	—
	IM2′	CBr	−0.9	4.2	13.9	—
	IM6	CBr	−0.9	4.2	13.9	—
	IM6′	CBr	−1.2	3.9	13.4	—
	IM3	CH	−1.2	−0.8	7.6	—
	IM3′	CH	−1.2	−0.8	7.6	—
	IM5	CH	−1.2	−0.8	7.6	—
	IM5′	CH	−1.2	−0.8	7.6	—
	IM4	CBr	−0.9	3.2	10.6	—
	IM4′	CBr	−0.9	3.2	10.5	—
H-abstraction from ethyl group	IM7-1	CH	−3.4	−1.0	8.7	−25.1
	IM7-2	CH	−3.4	−1.0	8.7	−25.1
	IM7′-1	CH	−3.4	−1.0	8.7	−25.1
	IM7′-2	CH	−3.4	−1.0	8.7	−25.1
H-abstraction from phenyl group	IM3-H	CH	−1.9	5.8	14.4	−5.9
	IM3′-H	CH	−1.9	5.8	14.4	−5.9
	IM5-H	CH	−1.9	5.8	14.4	−5.9
	IM5′-H	CH	−1.9	5.8	14.4	−5.9

[a] The species and sites correspond to the reaction pathways showed in Fig. 2. [b] ΔE_{RC}, ΔE_a and ΔE_{PC} were calculated at 0 K, and $\Delta G^{\ddagger}$ was calculated at 298 K.

Table 2 Calculated reaction rate constants (k_{OH}, cm^3 per molecule per s) and product branching ratio (Γ) for the reaction BTBPE + ·OH

Pathways	Species[a]	Sites[a]	k_{OH}[b]	Γ[b]
Addition to phenyl group	IM1 + IM1′	CO	1.4×10^{-14}	1.4%
	IM2 + IM2′ + IM6 + IM6′	CBr	0	0%
	IM3 + IM3′ + IM5 + IM5′	CH	7.4×10^{-13}	73.5%
	IM4 + IM4′	CBr	1.9×10^{-15}	0.2%
H-abstraction from ethyl group	IM7-1 + IM7′-1 + IM7-2 + IM7′-2	CH	2.5×10^{-13}	24.9%
H-abstraction from phenyl group	IM3-H + IM3′-H + IM5-H + IM5′-H	CH	3.4×10^{-16}	0%
Overall			1.0×10^{-12}	100%

[a] The species and sites correspond to the reaction pathways showed in Fig. 2 and Table 1. [b] k_{OH} and Γ were calculated at 298 K and 101 kPa.

transition states and intermediates involved in the reactions are shown in Fig. 6.

The reaction of IM3 with O_2 can proceed *via* direct H-abstraction to form hydroxylated BTBPE (OH-BTBPE) and O_2H or addition to form peroxyl radicals as other aromatic –OH adducts (*e.g.* benzene-OH and toluene-OH adducts).[54,55] Fig. 5A depicts the H-abstraction and addition pathways for the reaction IM3 + O_2 with corresponding ΔE_a and $\Delta G^{\ddagger}$ values, and relative energy (ΔE) and relative free energy values (ΔG) (to IM3 + O_2) of intermediates and products. For the H-abstraction process, O_2 could favorably abstract H atom at C site connecting –OH to form OH-BTBPE (P9) and O_2H radicals. The ΔE_a is 8.8 kcal mol^{-1}, corresponding to rate constant 2.2×10^{-21} cm^3 per molecule per s. However, H-abstraction at other sites could lead to thermodynamically unfeasible diradical products. The O_2 addition to IM3 should occur at the sites with high spin distribution, *i.e.* the *ortho*-carbon atoms (C2 and C4) and the *para*-carbon (C6) of the –OH position (shown in Fig. S2†), like cases of the reactions benzene-OH adducts + O_2 and BDE-OH adducts + O_2 since the triplet O_2 is diradical.[33,55] Also, O_2 can be added to the aromatic rings from the same or opposite side of the phenyl ring (*cis*- and *trans*-) with respect to the –OH group. A common feature for such additions is that ΔG values of all formed intermediates (IM8-IM13) are >0. ΔE_a value for *para*-addition at C6 site is lower than those of the other additions, indicating that *para*-addition at C6 site is most favorable.

The activated peroxy radicals (IM8–IM13) formed in the O_2 addition pathway could further transform, forming oxy hydroperoxide radical (finally leading to epoxy radicals) *via* H-shift and bicyclic radicals *via* cyclization, respectively.[54,55] The bicyclic radicals will exclusively recombine with O_2 to produce bicyclic peroxy radicals, then the bicyclic peroxy radicals are expected to react with NO to form the bicyclic alkoxy radicals which undergo ring cleavage finally as the reactions of other aromatics such as toluene.[54,56] However, some intermediates including IM9, IM11, IM12 and IM13 need to overcome high reaction barriers, and the others including IM8 and IM10 are thermodynamically unfeasible for further reactions. Therefore, due to higher energy of peroxy radicals relative to that of reactants IM3 + O_2 and hardly further transformation, the O_2 addition reaction could proceed reversibly, which is similar to the case for the reaction of the monoaromatic hydrocarbon-OH adducts such as benzene-OH, toluene-OH and chlorobenzene-OH with O_2.[54,55,57] As a result, O_2-addition rate constants are effectively assumed as the formation rate constant of products (P10–21). The calculated overall addition rate constant (Table

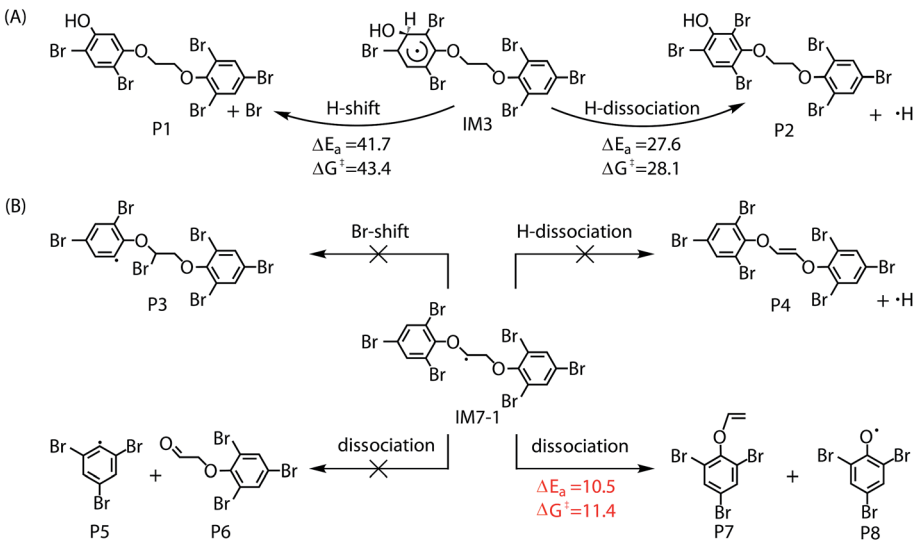

Fig. 4 Subsequent self-isomerization and dissociation pathways for IM3 (A) and IM7-1 (B).

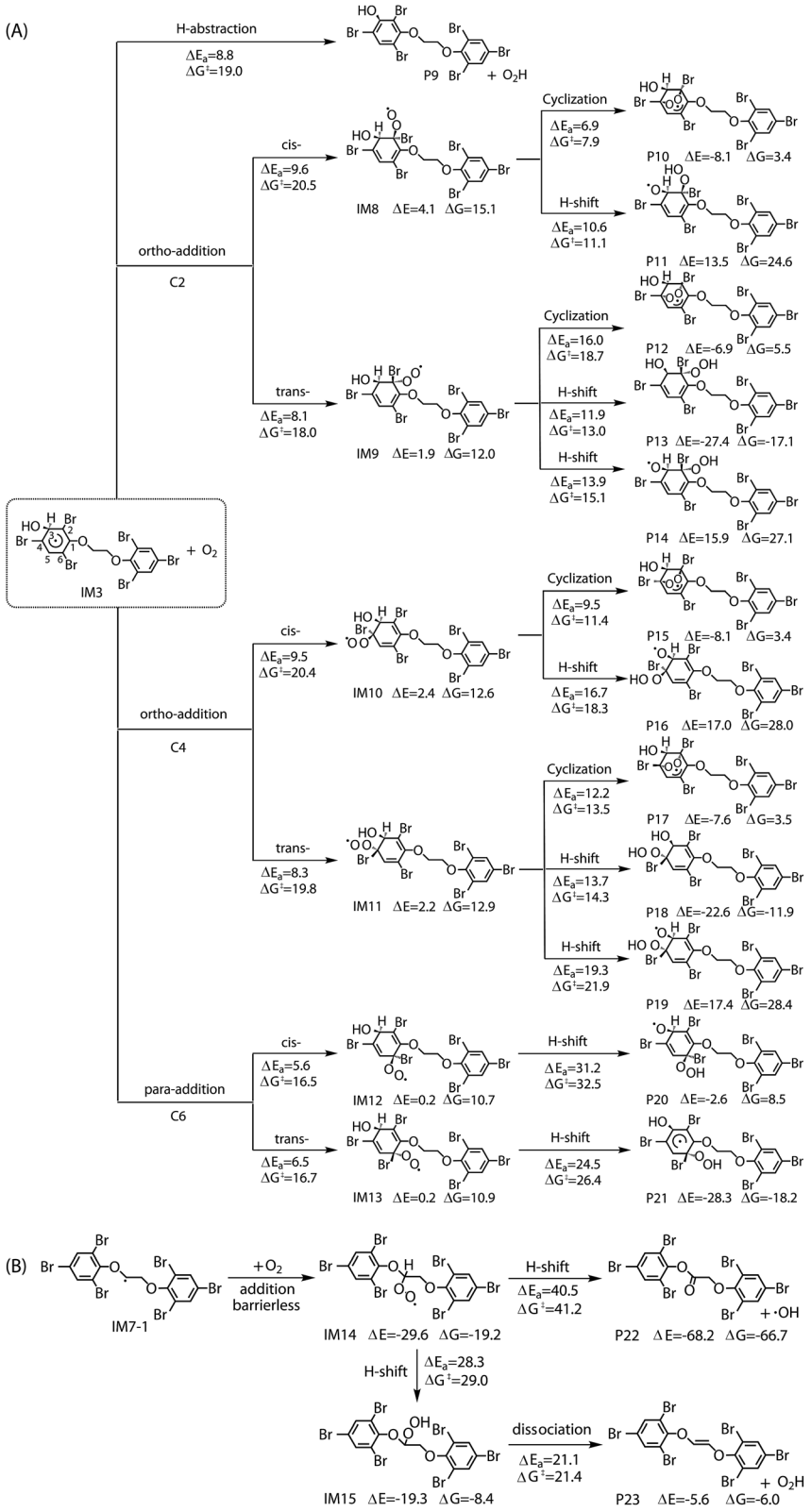

Fig. 5 Subsequent reaction pathways for IM3 (A) and IM7-1 (B) with O_2.

S3†) is 1.3×10^{-22} cm^3 per molecule per s, in which the *trans*-addition to C6 site forming P21 dominates the overall rate constant. In addition, the reaction rate constants for H-abstraction pathways, forming OH-BTBPE and O_2H radical, are higher than those for addition pathways. Thus, H-abstraction mainly contributes to final products for the

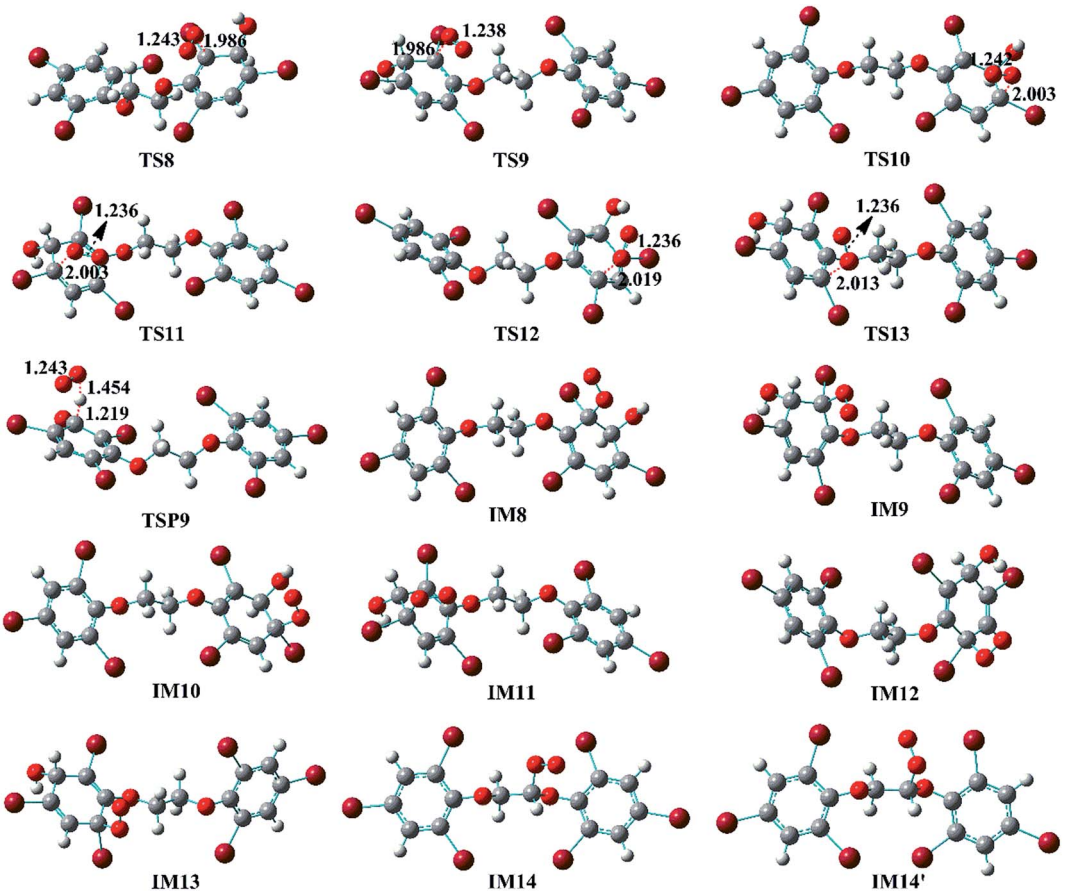

Fig. 6 PBE1PBE/6-31+G(d,p)-optimized geometries for some important transition states and intermediates involved in the reaction of IM3/IM7-1 + O_2. The distances are in angstroms (Å).

further transformation of IM3 in the presence of O_2, analogous to the reaction of OH adduct of PBDEs with O_2 to form OH-PBDEs.[52] Since high abundance of atmospheric O_2, the favorable H-abstraction pathway of IM3 with O_2 should have atmospheric importance even though its reaction energy barrier is relatively high. This also can be supported by the fact that pseudo-first order rate constant ($\sim 10^{-2}$ s^{-1}) of the H-abstraction is much higher than that ($\sim 10^{-4}$ s^{-1}) of collision controlled ·OH-molecule reactions that are of significance for the transformation of atmospheric pollutants.

Similar to the reactions of typical C-center radicals with O_2, O_2 can barrierlessly add to C7 site of IM7-1 to form the intermediate peroxy radicals (Fig. 5B). Peroxy radicals have two isomeric forms (IM14 and IM14′ in Fig. 6) owing to the different attacking direction of O_2. IM14 and IM14′ can easily interconvert with the approximate barrier 3 to 4 kcal mol^{-1}. For IM14, there are two possible H-transfer pathways. One is H-transfer from C7 site to OO site, which is followed by HO–O bond capture to form P18; the other is H-transfer from C7′ site to OO site to form oxy hydroperoxide radical (IM15), which can finally form P23 *via* HOO–C bond capture. The overall reaction energy barrier for latter pathway is much lower than that of former one, indicating the H-transfer from C7′ site to OO site to finally form P23 is most favorable for IM14. Based on the energetic information of the most favorable pathway, the calculated rate constant of IM7-1 + O_2 is 2.2×10^{-12} cm^3 per molecule per s. In addition, IM14 is an exclusive product with 100% product branching ratio. This should result from the fact that IM14 adduct lies in a deep well. We also note that an adduct formed in the reaction of other C-center radicals such as NH_2CHCH_2OH with O_2,[58] can easily further transform to fragmental products, which is different from IM7-1 + O_2. The steric or electronic effect of Br near the reactive center could be a possible reason for the difference.

3.5. Fate of primary intermediates

To discuss the final fate of primary intermediates (IM3 and IM7-1) formed by BTBPE + ·OH in the atmosphere, we evaluate the competition of their different transformation pathways, including self-isomerization/dissociation, bimolecular reactions with O_2/NO. To effectively compare the competition of these pathways, bimolecular rate constants for IM3/IM7-1 + O_2 and IM3/IM7-1 + NO were multiplied by the concentration of O_2 (4.92×10^{18} molecules cm^{-3}) and NO ($\sim$5 ppb, 2.69×10^{10} molecules cm^{-3}), respectively, to obtain theirs pseudo-first order rate constants. The reaction rate constant for the

reaction of IM3 with NO is assumed in the order of 10^{-14} cm^3 per molecule per s based on the reaction of typical aromatic-OH adducts with NO,[59] and IM7-1 + NO in the order of 10^{-12} cm^3 per molecule per s based on the reaction rate constant of $\cdot CH_2OCH_3$ with NO.[60] In addition, to evaluate final yield of products, a comprehensive product branching ratio was determined by calculating the product of branching ratio of IM3 and IM7-1 in the ·OH initiated reaction and branching ratio of products of their subsequent reactions, respectively. The rate constants of all pathways and the comprehensive product branching ratio were listed in Table S3† and Fig. 7, respectively. The main fate of IM3 and IM7-1 was presented in Fig. 7A and B, respectively.

For IM3, as can be seen in Fig. 7A, the pseudo-first order rate constant ($\sim 10^{-2}$ s^{-1}) with O_2 is much higher than that ($\sim 10^{-4}$ s^{-1}) with NO and its unimolecular self-isomerization/dissociation rate constant ($\sim 10^{-8}$ s^{-1}). The yield of the OH-BTBPE forming from oxidation of BTBPE is about 72.3%, which indeed is the main product. Similar to IM3, the pseudo-first order rate constant ($\sim 10^{7}$ s^{-1}) of IM7-1 with O_2 is much higher than that ($\sim 10^{-2}$ s^{-1}) with NO and its unimolecular self-dissociation rate constant ($\sim 10^{4}$ s^{-1}). It deserves mentioning that unimolecular self-dissociation rate constant of IM7-1 is much higher than that of reaction of IM7-1 with NO, which is different from the case of IM3. The yield of peroxy radicals from the reaction IM7-1 + O_2 is estimated to be 24.8%. Based on above discussions, we can conclude that OH-BTBPE and peroxy radicals, are the main fate of primary intermediates formed by BTBPE + ·OH in the atmosphere. In addition, pseudo-first order rate constant of IM3 and IM7-1 with O_2 is higher than that ($\sim 10^{-6}$ s^{-1}, [OH] is 9.7×10^5 molecules cm^{-3}) of the initial reaction BTBPE + ·OH, indicating the reaction of ·OH with BTBPE is the rate determining step in ·OH initiated reaction of BTBPE.

3.6. Conclusions and atmospheric implications

The atmospheric oxidation mechanism and kinetics of BTBPE initiated by ·OH was investigated by a combined quantum chemical method and kinetics modeling. The initial oxidation proceeds *via* the ·OH addition and hydrogen abstraction pathways to form intermediates (IM7-1 and IM3), which can further react with O_2 to finally form peroxy radicals and OH-BTBPE. The Daphnia Magna LC50 (48 h) values for OH-BTBPE are predicted to be obviously higher than those for BTBPE (details presented in Table S4†). Therefore, formed OH-BTBPE tends to be more toxic than their parent compound BTBPE, which could increase the environmental risk of BTBPE emission and deserve further investigation. This is similar to previous findings that most hydroxylated brominated aromatics are of higher toxicity than themselves, for instance, OH-PBDEs and bromophenol have been proved to be more toxic than PBDEs and bromobenzene, respectively.[61,62] The calculated overall reaction rate constant is 1.0×10^{-12} cm^3 per molecule per s, translating 11.8 days atmospheric lifetime ($\tau = 1/k_{OH}[OH]$) of BTBPE. Although the lifetime of BTBPE is much lower than that (around hundreds days) of the banned PBDEs (pentaBDE, octaBDE and decaBDE), the substitute of PBDEs by BTBPE still has atmospheric persistence.[52,63–65] In addition, it deserves mentioning that heterogeneous reactions of BTBPE on atmospheric particles will affect its overall atmospheric lifetime since BTBPE is a semi-volatile compound. Therefore, the effect of other particles such as black carbon, mineral dust on the lifetime of BTBPE deserves future investigation. Our study lays a good foundation for the future study on heterogeneous reactions of BTBPE.

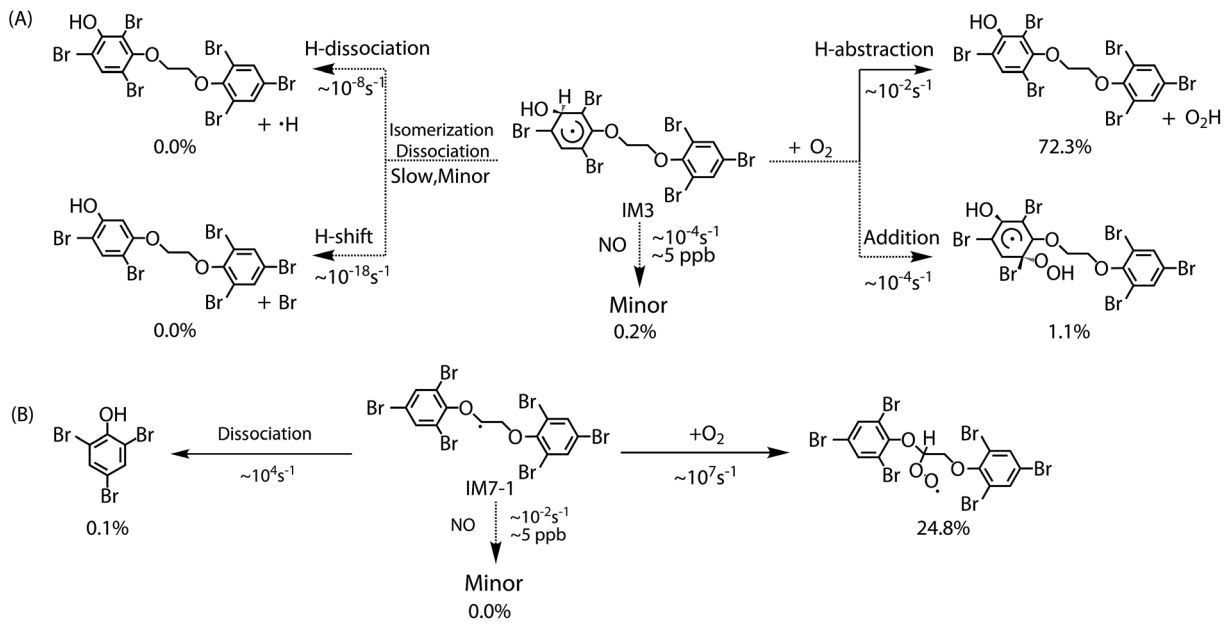

Fig. 7 Summary for the fate of primary intermediates IM3 (A) and IM7-1 (B). The width of the arrows indicates the relative importance of the reaction pathway. Percentage under different products indicates their respective final yield.

Acknowledgements

We thank Prof. John R. Barker (University of Michigan) for providing the MultiWell-2014.1 program. The study was supported by the National Natural Science Foundation of China (21477015, 21325729), Major International (Regional) Joint Research Project (21661142001) and the Fundamental Research Funds for the Central Universities.

References

1 A. Bergman, J. Heindel, S. Jobling, K. Kidd and R. T. Zoeller, *State of the science of endocrine disrupting chemicals*, 2012, http://www.unep.org/pdf/9789241505031_eng.pdf.
2 United Nations Environment Programme (UNEP), *DTI/1639/GE, Global chemicals outlook-Towards sound management of chemicals*, ISBN: 978-92-807-3320-4, 2013, https://wedocs.unep.org/rest/bitstreams/14105/retrieve.
3 Stockholm Convention, *The list of POPs in the Stockholm Convention*, http://chm.pops.int/TheConvention/ThePOPs/ListingofPOPs/tabid/2509/Default.aspx.
4 Regulation (EC) No 1907/2006 of the European Parliament and of the Council of 18 December 2006 concerning the Registration, Evaluation, Authorisation and Restriction of Chemicals (REACH), establishing a European Chemicals Agency, amending Directive 1999/45/EC and repealing Council Regulation (EEC) No 793/93 and Commission Regulation (EC) No 1488/94 as well as Council Directive 76/769/EEC and Commission Directives 91/155/EEC, 93/67/EEC, 93/105/EC and 2000/21/EC (OJ L 396, 30.12.2006).
5 J. B. Zimmerman and P. T. Anastas, *Science*, 2015, **347**, 1198–1199.
6 K. Kim, Z. Shon, H. T. Nguyen and E. Jeon, *Atmos. Environ.*, 2011, **45**, 1369–1382.
7 B. O. Bolaji and Z. Huan, *Renewable Sustainable Energy Rev.*, 2013, **18**, 49–54.
8 D. Chen, K. Kannan, H. Tan, Z. G. Zheng, Y. L. Feng, Y. Wu and M. Widelka, *Environ. Sci. Technol.*, 2016, **50**, 5438–5453.
9 E. Hoh, L. Y. Zhu and R. A. Hites, *Environ. Sci. Technol.*, 2005, **39**, 2472–2477.
10 Organisation for Economic Co-operation and Development (OECD), *The 2007 OECD list of high production volume chemicals*, Environment, Health and Safety Publications, Series on Testing and Assessment, No. 112, 2009, http://www.oecd.org_officialdocuments_publicdisplaydocumentpdf__cote=env_jm_mono(2009)40&doclanguage=en.
11 A. Covaci, S. Harrad, M. A. Abdallah, N. Ali, R. J. Law, D. Herzke and C. A. de Wit, *Environ. Int.*, 2011, **37**, 532–556.
12 H. M. Stapleton, J. G. Allen, S. M. Kelly, A. Konstantinov, S. Klosterhaus, D. Watkins, M. D. Mcclean and T. F. Webster, *Environ. Sci. Technol.*, 2008, **42**, 9455–9456.
13 M. J. L. Guardia and R. C. Hale, *Environ. Int.*, 2015, **79**, 106–114.
14 A. Salamova and R. A. Hites, *Environ. Sci. Technol.*, 2011, **45**, 8698–8706.
15 H. Qi, W. Li, L. Liu, W. Song, W. Ma and Y. Li, *Sci. Total Environ.*, 2014, **491–492**, 60–66.
16 K. Vorkamp, R. Bossi, F. F. Riget, H. Skov, C. Sonne and R. Dietz, *Environ. Pollut.*, 2015, **196**, 284–291.
17 K. Arinaitwe, D. C. Muir, B. T. Kiremire, P. Fellin and H. Li, *Environ. Sci. Technol.*, 2014, **48**(3), 1458–1466.
18 M. Shoeib, L. Ahrens, L. M. Jantunen and T. Harner, *Atmos. Environ.*, 2014, **99**, 140–147.
19 Y. Ma, A. Salamova, M. Venier and R. A. Hites, *Environ. Sci. Technol.*, 2013, **47**, 11457–11464.
20 E. D. Schreder and M. J. L. Guardia, *Environ. Sci. Technol.*, 2014, **48**, 11575–11583.
21 E. F. Davis, S. L. Klosterhaus and H. M. Stapleton, *Environ. Int.*, 2012, **40**, 1–7.
22 R. Yang, H. Wei, J. Guo and A. Li, *Environ. Sci. Technol.*, 2012, **46**, 3119–3126.
23 K. Vorkamp and F. F. Rigét, *Chemosphere*, 2014, **111**, 379–395.
24 C. A. D. Wit, D. Herzke and K. Vorkamp, *Sci. Total Environ.*, 2010, **408**, 2885–2918.
25 A. Möller, Z. Xie, M. Cai, G. Zhong, P. Huang, M. Cai, R. Sturm, J. He and R. Ebinghaus, *Environ. Sci. Technol.*, 2011, **45**, 6793–6799.
26 H. Hakk and R. J. Letcher, *Environ. Int.*, 2003, **29**, 801–828.
27 Y. N. Zhang, J. Chen, Q. Xie, Y. Li and C. Zhou, *Chemosphere*, 2016, **150**, 453–460.
28 M. Altarawneh and B. Z. Dlugogorski, *Environ. Sci. Technol.*, 2014, **48**, 14335–14343.
29 M. Altarawneh and B. Z. Dlugogorski, *Environ. Sci. Technol.*, 2013, **47**, 5118–5127.
30 M. Altarawneh and B. Z. Dlugogorski, *Chemosphere*, 2014, **114**, 129–135.
31 M. Altarawneh and B. Z. Dlugogorski, *J. Phys. Chem. A*, 2014, **118**, 9338–9346.
32 J. D. Raff and R. A. Hites, *J. Phys. Chem. A*, 2006, **110**, 10783–10792.
33 H. Cao, M. He, D. Han, J. Li, M. Li, W. Wang and S. Yao, *Environ. Sci. Technol.*, 2013, **47**, 8238–8247.
34 J. Zhou, J. Chen, C. H. Liang, Q. Xie, Y. N. Wang, S. Zhang, X. Qiao and X. Li, *Environ. Sci. Technol.*, 2011, **45**, 4839–4845.
35 M. J. Frisch, G. W. Trucks, H. B. Schlegel, G. E. Scuseria, M. A. Robb, J. R. Cheeseman, *et al.*, *Gaussian 09*, Gaussian, Inc., Wallingford, CT, 2009.
36 G. P. Wood, A. Sreedhara, J. M. Moore and B. L. Trout, *J. Phys. Chem. A*, 2014, **118**, 2667–2682.
37 Y. Zhao and D. Truhlar, *Theor. Chem. Acc.*, 2008, **120**, 215–241.
38 J. R. Barker, *Int. J. Chem. Kinet.*, 2009, **41**, 748–763.
39 J. R. Barker, *Int. J. Chem. Kinet.*, 2001, **33**, 232–245.
40 J. R. Barker, N. F. Contributors Ortiz, J. M. Preses, L. L. Lohr, A. Maranzana, P. J. Stimac, T. L. Nguyen and T. J. D. Kumar, *MultiWell-2014.1 Software*, Universityof Michigan, Ann Arbor, MI, 2014.
41 J. R. Barker and N. F. Ortiz, *Int. J. Chem. Kinet.*, 2001, **33**, 246–261.
42 P. J. Robinson and K. A. Holbrook, *Unimolecular Reactions*, John Wiley & Sons, New York, 1972.
43 C. Eckart, *Phys. Rev.*, 1930, **35**(11), 1303–1309.

44 R. G. Gilbert and S. C. Smith, *Theory of unimolecular and recombination reactions*, Blackwell Scientific Publications, Carlton, Australia, 1990.
45 K. G. Joback and R. C. Reid, *Chem. Eng. Commun.*, 2007, **57**, 233–243.
46 J. R. Barker, N. F. Ortiz, J. M. Preses, L. L. Lohr, A. Maranzana, P. J. Stimac, T. L. Nguyen and T. J. Dhilip Kumar, *MultiWell Program Suite User Manual, (MultiWell-2014.1)*, http://aoss-research.engin.umich.edu/multiwell/.
47 Y. Georgievskii and S. J. Klippenstein, *J. Chem. Phys.*, 2005, **122**, 194103.
48 H. B. Xie, F. F. Ma, Y. Wang, N. He, Q. Yu and J. W. Chen, *Environ. Sci. Technol.*, 2015, **49**, 13246–13255.
49 C. Lee, W. T. Yang and R. G. Parr, *Phys. Rev. B: Condens. Matter Mater. Phys.*, 1988, **37**, 785–789.
50 R. Ahlrichs, M. Bär, M. Häser, H. Horn and C. Kölmel, *Chem. Phys. Lett.*, 1989, **162**, 165–169.
51 H. Cao, M. He, D. Han, Y. Sun and J. Xie, *Atmos. Environ.*, 2011, **45**, 1525–1531.
52 H. Cao, D. Han, M. Li, X. Li, M. He and W. Wang, *J. Phys. Chem. A*, 2015, **119**, 6404–6411.
53 Y. R. Luo, *Handbook of bond dissociation energies in organic compounds*, Crc Press Inc., 2003, pp. 39–69.
54 I. Suh, R. Zhang, L. T. Molina and M. J. Molina, *J. Am. Chem. Soc.*, 2003, **125**, 12655–12665.
55 D. R. Glowacki, L. M. Wang and M. J. Pilling, *J. Phys. Chem. A*, 2009, **113**, 5385–5396.
56 R. Wu, S. Pan, Y. Li and L. Wang, *J. Phys. Chem. A*, 2014, **118**, 4533–4547.
57 R. Wu, S. Wang and L. Wang, *Chemosphere*, 2014, **111**, 537–544.
58 H. B. Xie, C. Li, N. He, C. Wang, S. Zhang and J. Chen, *Environ. Sci. Technol.*, 2014, **48**, 1700–1706.
59 R. Koch, R. Knispel, M. Elend, M. Siese and C. Zetzsch, *Atmos. Chem. Phys.*, 2007, **7**, 2057–2071.
60 M. Rissanen, M. Ihlenborg, T. T. Pekkanen and R. S. Timonen, *J. Phys. Chem. A*, 2015, **119**, 7734–7741.
61 A. R. Zota, J. S. Park, Y. Wang, M. Petreas, R. T. Zoeller and T. J. Woodruff, *Environ. Sci. Technol.*, 2011, **45**, 7896–7905.
62 J. Jiang, Y. Gao, S. Y. Pang, Q. Wang, X. Huangfu, Y. Liu and J. Ma, *Environ. Sci. Technol.*, 2014, **48**, 10850–11088.
63 European Union, Directive 2002/95/EC of the European Parliament and of the Council on the restriction of the use of certain hazardous substances in electrical and electronic equipment, Off J Eur Union, 2003, vol. 37, pp. 19–23.
64 European Court of Justice, Cases C-14/06 and C-295/06, Judgement of the Court, 1 April 2008, Directive 2002/95/EC and Commission Decision 2005/717/EC, 2008Error! Hyperlink reference not valid. http://curia.europa.eu, accessed, July 2010.
65 I. Liagkouridis, A. P. Cousins and I. T. Cousins, *Sci. Total Environ.*, 2015, **524**, 416–426.

